SAND2015-20736J

Radiative Lifetimes of Zincblende CdSe/CdS Quantum Dots

Ke Gong[a], James E. Martin[b], Lauren E. Shea-Rohwer[b], Ping Lu[b] and David F. Kelley*[a]

[a] *Chemistry and Chemical Biology, University of California Merced, 5200 North Lake Road, Merced, CA 95343*

[b] *Sandia National Laboratories, P.O. Box 5800, MS-0892, Albuquerque, NM 87185-0892*

Abstract.

Recent synthetic advances have made available very monodisperse zincblende CdSe/CdS quantum dots having near-unity photoluminescence quantum yields. Because of the absence of nonradiative decay pathways, accurate values of the radiative lifetimes can be obtained from time-resolved PL measurements. Radiative lifetimes can also be obtained from the Einstein relations, using the static absorption spectra and the relative thermal populations in the angular momentum sublevels. One of the inputs into these calculations is the shell thickness, and it is useful to be able to determine shell thickness from spectroscopic measurements. We use an empirically-corrected effective mass model to produce a "map" of exciton wavelength as a function of core size and shell thickness. These calculations use an elastic continuum model and the known lattice and elastic constants to include the effect of lattice strain on the band gap energy. The map is in agreement with the known CdSe sizing curve and with the shell thicknesses of zincblende core/shell particles obtained from TEM images. If selenium-sulfur diffusion is included and lattice strain is omitted then the resulting map is appropriate for wurtzite CdSe/CdS quantum dots synthesized at high temperatures, and this map is very similar to one previously reported (Embden*, et al.*, *J. Am. Chem. Soc.* **2009,** 131, 14299). Radiative lifetimes determined from time resolved measurements are compared to values obtained from the Einstein relations, and found to be in excellent agreement. Radiative lifetimes are found to decrease with shell thickness, similar to the size dependence of one-component CdSe quantum dots and in contrast to the size dependence in type-II quantum dots.

Introduction.

Quantum dots (QDs) are of great interest because of their tunable and intense photoluminescence (PL). Very high PL quantum yields and photostability are often obtained from CdSe/CdS core/shell QDs, making them of particular interest. CdSe/CdS core/shell nanocrystals have optical properties that are unique amongst semiconductor QDs and have been extensively studied. Most of these particles are synthesized at high temperatures and have a wurtzite crystal structure, which is the most stable form. Although these core/shell QDs typically have high PL quantum yields when shells are thin (a few CdS layers), the quantum yields drop with increasing shell thickness.[1] Recently Nan *et al*. reported a low temperature synthesis of very high quality zincblende CdSe/CdS core/shell QDs.[2] The PL quantum yields of these QDs is very high and remains high for relatively thick shells. The reason for the differences in the optical properties is that the "synthetic philosophy" for these particles is entirely different than that underlying previous syntheses giving wurtzite particles.

In most syntheses of wurtzite core/shell particles, shell growth is done using a SILAR procedure at fairly high temperatures, > 200 C°.[3-5] There are two reasons for this. First, the high temperatures are needed for the reaction of the cadmium and sulfur precursors to proceed at a reasonable rate; and second, the higher temperatures permit in-situ particle annealing, resulting in better crystallinity. Successive addition of cadmium and sulfur precursors can produce very thick CdS shells, the so-called "giant" nanocrystals.[6, 7] The main problem with this approach is that there is a 4% lattice mismatch between CdSe and CdS that results in considerable lattice strain at the core-shell interface.[8] This strain can be relieved by shell surface reconstruction which readily proceeds above about 200 °C. The result is that the shells are typically irregular and have many surface defects.[9] These defects can act as electron-hole recombination centers, lowering the PL quantum yield.

In contrast, in the recent zincblende synthesis, shell deposition proceeds from a very reactive single CdS precursor[2] at relatively low temperatures, < 160 °C. Surface reconstruction is an activated process and does not readily occur at such low temperatures.[9] The result is that the zincblende core/shell particles are metastable with respect to lattice-strain-induced shell defects and have much more uniform and closer to defect free shells than the corresponding wurtzite particles. This results in very high PL quantum yields, even for particles with comparatively thick shells. The original reports give the PL quantum yields of about 85%. We have optimized this synthesis and get quantum yields of about 95%. Zincblende CdSe/CdS QDs are also quite stable and it seems that these particles hold great promise for applications in photovoltaics and especially light emitting diodes.

Having accurate radiative lifetimes is fundamental to understanding the luminescence of any type of QD. Radiative lifetimes are, in principle, easy to obtain. One simply measures the PL decay kinetics, and in the absence of nonradiative decay pathways, the measured decay time is the radiative lifetime. However, the observed PL QYs of most types of QDs are far below unity, indicating that non-radiative processes compete with luminescence and cannot be ignored. The observed PL decay rate is the sum of the radiative and nonradiative rates, and different fractions of the sample having different nonradiative rates can make the interpretation of multi-exponential PL decay kinetics ambiguous and problematic.[10]

Radiative rates can also be calculated from absorption spectra using the Einstein relations.[11, 12] Specifically, for a II-VI QD the relation is

$$A = \frac{8\pi\ 0.2303 C_{fs} n_f^3}{N_a c^2 n_a} \left\langle \nu_f^{-3} \right\rangle^{-1} \int \frac{\varepsilon(\nu)}{\nu} d\nu \approx 2.88 x 10^{-9} C_{fs} n^2 \left\langle \tilde{\nu}_f^2 \right\rangle \int \varepsilon(\tilde{\nu}) d\tilde{\nu} \qquad \text{equation 1.}$$

where N_a is Avogadro's number, c is the speed of light, $\varepsilon(\nu)$ is the molar extinction coefficient (L mol^{-1} cm^{-1}) at frequency ν, ν_f ($\tilde{\nu}_f$) is the fluorescence frequency (wavenumber), brackets denote an averaged quantity, C_{fs} is a factor related to the relative populations in the dark and bright fine structure levels (discussed below) and n_a and n_f are the refractive indices of the surrounding solvent at the absorption and luminescence wavelengths, respectively. In the case where the absorption and luminescence spectra are narrow and there is minimal Stokes shift, the left part of equation 1 simplifies to the right part, with $n = n_a = n_f$. Alternatively, the radiative rate may be given in terms of the oscillator strength of the transition, f

$$A = \frac{2\pi n e^2 \nu^2}{\varepsilon_0 m c^3} C_{fs} f \qquad \text{equation 2.}$$

where f is given by

$$f = \frac{4m\nu}{e^2} \frac{0.2303\, nc\varepsilon_0}{N_a} \int \frac{\varepsilon(\nu)}{\nu} d\nu \qquad \text{equation 3.}$$

These expressions ignore local field effects, which enter into expressions for the absorption and luminescence in the same way, and therefore cancel.

Equations 1 – 3 are the usual expressions for the radiative lifetime, except for the inclusion of the factor that takes into account thermal populations in the angular momentum fine structure, C_{fs}. This factor is given by[10]

$$C_{fs} = \frac{\sum_i f_i \exp(-E_i / k_B T)}{\sum_i \exp(-E_i / k_B T)} \qquad \text{equation 4.}$$

where k_B is the Boltzmann constant, E_i and f_i are the energy and fraction of the total absorption oscillator strength in the *i-th* transition, respectively. There are eight thermally accessible angular momentum sublevels in the $1S_e$-$1S_{3/2}$ exciton. Rapid equilibration with the population of the dark states effectively increases the radiative lifetime compared to the case of a single absorbing and emitting oscillator. This is not a small effect; in the absence of crystal field or shape anisotropy mixing, five of the eight fine structure sublevels are dark. Following photon absorption, rapid relaxation occurs amongst the bright and dark states and luminescence comes from a temperature-dependent distribution of states, each having its own radiative rate. The energies and oscillator strengths of these different angular momentum sublevels depend of the size, shape and crystal structure of the QD. These energy separations are comparable to kT at room temperature and there is a Boltzmann distribution of populations in these different states, complicating the evaluation of C_{fs}. Accurate calculation of radiative lifetimes requires that the values of the PL energy, the integrated extinction coefficient and C_{fs} be considered.

In this paper we examine the radiative lifetimes of a series of CdSe/CdS core/shell particles having different shell thicknesses. These values are obtained directly from time-resolved measurements and compared to values obtained from static spectra and the evaluation of equation 1 or 2. Agreement between values obtained from these completely different approaches is very good, indicating that the factors controlling the radiative lifetime are well understood.

Results and Discussion.

Absorption (molar extinction coefficient) and PL spectra of the zincblende CdSe core and CdSe/CdS core/shell QDs are shown in figures 1 and 2. The extinction coefficient spectra shown in figure 1 are determined from raw absorption spectra.

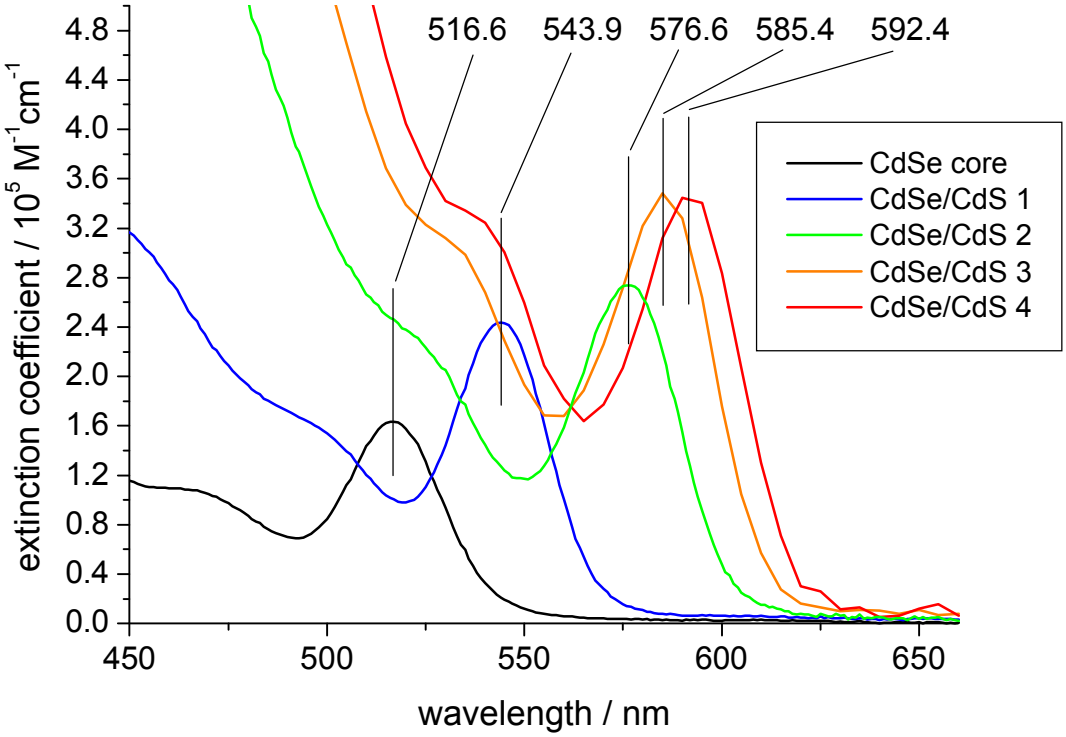

Figure 1. Absorption spectra of 2.64 nm zincblende CdSe QDs and corresponding core/shell particles having shell thicknesses of 0.00, 0.39, 1.10, 1.52, and 2.00 nm, as indicated.

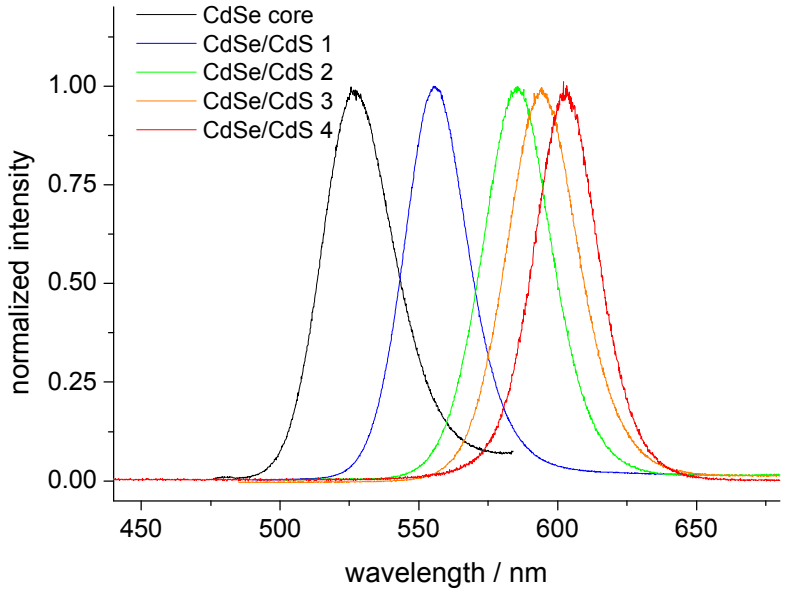

Figure 2. Normalized photoluminescence spectra of the same QDs as in figure 1.

The outline of the procedure for doing this in the absence of direct concentration determinations is the following. We initially determine exciton energy as a function of core size and shell thickness, making a "map" of exciton wavelength for CdSe/CdS core/shell particles. This is useful because it enables spectroscopic determination of shell thickness for particles for which TEM data are not available. The core diameter and shell thickness results are used along with the known bulk CdSe, CdS and solvent absorption coefficients and refractive indices to obtain extinction coefficients at a wavelength where quantum confinement effects are negligible, in this case, 350 nm. Knowing the extinction coefficient at this wavelength directly converts an absorption spectrum to an extinction coefficient spectrum. The extinction coefficient spectra are then used to obtain absolute oscillator strengths and radiative lifetimes using equations 1 – 4.

1. Exciton energy as a function of core size and shell thickness.

The size-dependent spectroscopy of wurtzite versus zincblende CdSe particles has not been extensively studied, but indications are that the crystal structure makes little difference in the effects of quantum confinement. This is not surprising, as the energetic difference between the two forms is very small, 1.4 meV per CdSe. We therefore assume that size calibration curves obtained for wurtzite may also be applied to zincblende particles. The cores have an absorption maximum at 516.6 nm, see figure 1. Using the well-established sizing curve for CdSe particles,[13] this corresponds to 2.64 nm diameter particles. A TEM image of the core/shell particles having an absorption maximum at 592.4 nm (indicated as CdSe/CdS 4 in figures 1 and 2) is shown in figure 3.

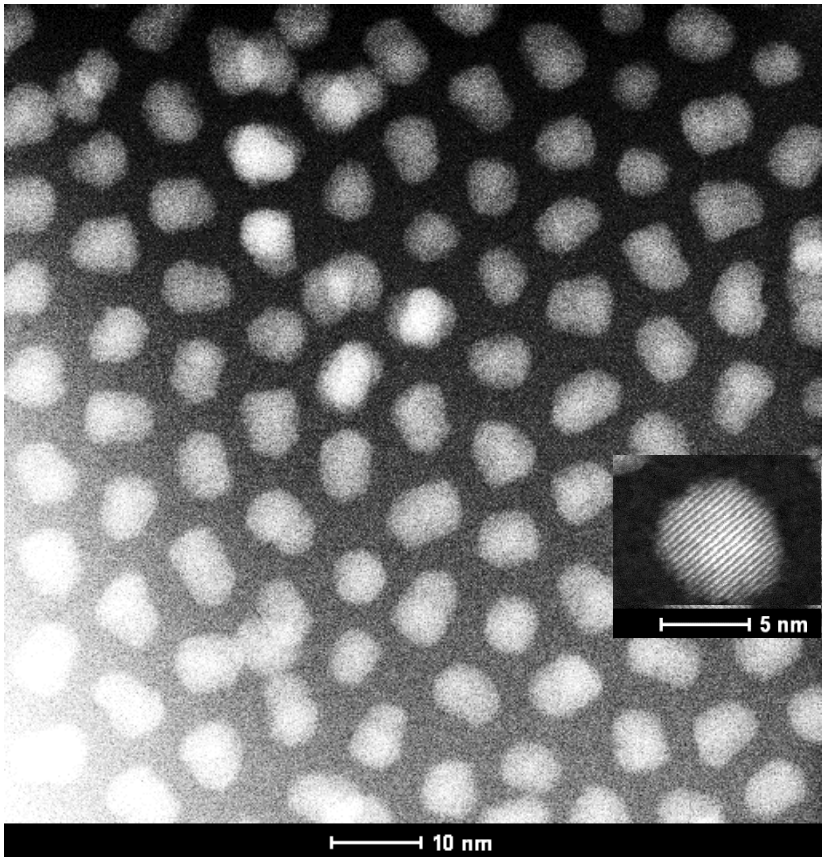

Figure 3. TEM image of the core/shell particles having an absorption maximum at 592.4 nm. The inset shows a typical high resolution image.

The particles are somewhat non-spherical, having dimensions varying from about 6.2 to 9.0 nm. The ensemble average dimension is obtained from the measurement of many particles and is found to be 6.6 nm. With the known core diameter of 2.64 nm, these images indicate that for these particles the average shell thickness is 2.0 nm. The shift of the lowest exciton wavelength from 516.6 to 592.4 nm constrains the calculation of any core/shell sizing map.

The approach used here to generate this map is based on the known CdSe sizing curve and calculation of the exciton energies using effective mass approximation (EMA) wavefunctions. Wurtzite and zincblende CdSe have very similar spectroscopic energetic and properties and we make the assumption that the wurtzite CdSe sizing curve can also be used for zincblende particles. EMA calculations are known to predict larger quantum confinement effects than what is observed. These errors are minimized by considering the electron and hole moving in potentials having finite barriers at the particle surface. However, even with finite barriers, EMA calculations typically over-predict the extent of quantum confinement, and the extent of these errors increases with increasing quantum confinement energy. The fundamental problem is that the effective mass is defined as $m^* = \hbar^2 \left(\frac{\partial^2 E}{\partial k^2} \right)^{-1}$, and the plot of E versus k is not quadratic at the larger quantum confinement energies of the smaller particles.[14, 15] The obvious solution to this problem is to empirically correct the effective masses as a function of quantum confinement energy, and that is the approach taken here. Since most of the quantum confinement is in the conduction band electron, this empirical correction is applied only to the electron effective mass. Applying a correction to the electron effective mass means that the total quantum confinement energy depends on the electron effective mass and vice-versa. It follows that the correction factor to the electron effective mass must be calculated in a way that is self-consistent with the calculated quantum confinement energies. Throughout these calculations, the electron-hole coulombic interaction is treated as a perturbation. We find that the corrected electron effective mass may be given by, $m_e^*(corrected) = m_e^*(bulk)\left(0.36773 + 2.75634x10^{-4} E_{QC} - 8.3105x10^{-9} E_{QC}^2\right)$, where E_{QC} is the electron plus hole quantum confinement energy. The way this is implemented is to start out assuming the low energy (bulk) electron effective mass, calculate electron and hole quantum confinement energies, use these quantum confinement energies to get a corrected electron effective mass, and so on. This procedure converges to self-consistent values in a few iterations. This empirical correction is chosen so that the EMA calculations very accurately reproduce the known CdSe sizing curve for particles having exciton wavelengths of 500 – 650 nm.[13]

These calculations are also applied to CdSe/CdS core/shell particles. This extension is non-trivial for two reasons. First, the presence of core/shell lattice mismatch, and second, the possibility of selenium and sulfur interdiffusion. Diffusion is a strongly activated process and appropriate to the low-temperature shell deposition conditions used here, we will initially ignore radial diffusion. The lattice parameter of CdSe is about 4% larger than for CdS, and the core-shell lattice mismatch results in the core being under isotropic pressure and the shell being under radial pressure and tangential tension.[16, 17] These strains affect the respective conduction band energies, which is taken into account through an elastic continuum calculation using the known elastic parameters of each material.[18-20] This calculation gives the volumetric strain as a function of radial position. This result, when combined with the volume dependent conduction

band energy shifts, allows calculation of an accurate conduction band radial potential, as was done in reference 21. The valence band potential is much less affected by strain, and is taken to be bulk values. Electron and hole wavefunctions are calculated using these potentials. A crucial parameter in the electron wavefunction calculation is the zero-strain CdSe-CdS conduction band offset, which is estimated to be between 0 and 0.3 eV.[22-24] If this is taken to be 0.047eV and the same electron effective mass correction factor is applied to the CdS conduction band electron, then this EMA calculation also accurately gives the exciton energy of the 6.6 nm core/shell particles, see figures 1 and 3. This approach has been used to calculate the exciton energies of a wide range of cores sizes and shell thicknesses. A map of the exciton energy as a function of core size and shell thickness is shown in figure 4 and in the Supporting Information. The elastic continuum model is not a good approximation for very thin shells, (less than a full monolayer) and calculations for those particles are omitted.

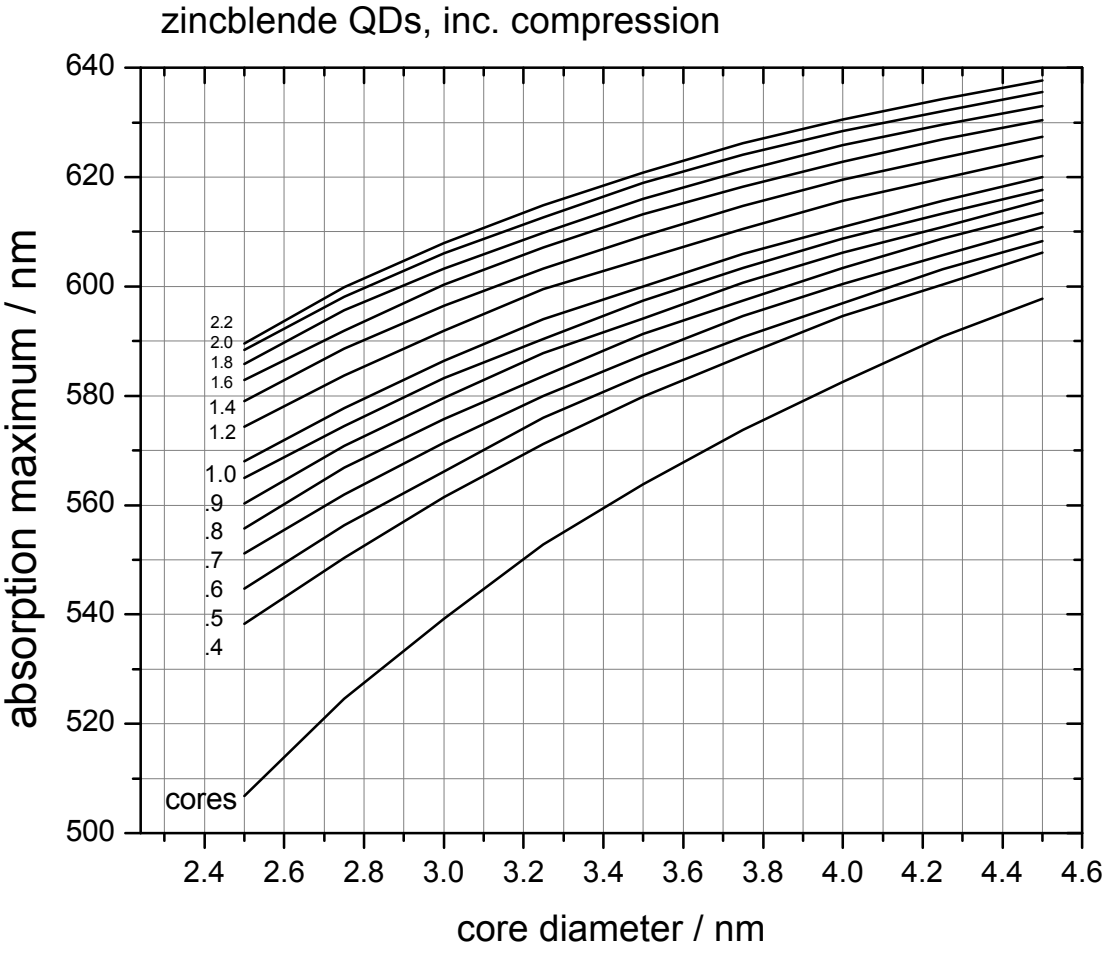

Figure 4. Exciton wavelength map assuming no core-shell interdiffusion and core compression calculated with bulk elastic parameters. The calculations assume smooth shells and a coherent core/shell interface.

The map in figure 4 assumes both a coherent core-shell interface and a uniform shell thickness, resulting in significant strain-induced spectral shifts. These are good assumptions for the zincblende particles for which the shell has been grown at low temperature. However, much of the lattice strain energy is released upon forming a rough shell and this occurs when thick wurtzite shells are grown at high temperatures and/or subsequently annealed.[9] In addition to relieving much of the lattice strain, high temperature shell deposition and subsequent annealing results in significant radial diffusion of the selenium and sulfur across the core-shell interface. This diffusion has the effect of changing both the conduction and, especially, valence band radial potentials. Thus, the effect of annealing is that the conduction band potential is altered by the graded composition and the loss of volumetric lattice strain. The valence band potential is not greatly affected by volumetric strain, but is affected by the change in composition profile. Valence band energies change nonlinearly with composition, a phenomenon referred to as "optical band-bowing," and this effect is included in the calculation of the valence band radial potential.[25-27] These considerations are relevant to the results on wurtzite CdSe/CdS particles reported in reference 5. In these studies, the CdS shells were grown at relatively high temperature and subsequently annealed at 200 °C. In contrast, the particles used here are zincblende and with the shells grown at much lower temperatures, <160 °C, and do not readily undergo surface reconstruction. They have more uniform shell thicknesses and are metastable with respect to release of the lattice strain and shell roughening. The present zincblende core/shell particles may therefore be expected to have somewhat different spectroscopic properties than the particles studied in reference 5. Using the same CdSe and CdS valence and conduction band potentials, we have also calculated core/shell exciton wavelengths maps for the case of no core compression, with and without radial interdiffusion. These radial composition profiles are obtained by solving the radial diffusion equation, as explained in reference 21. The valence and conduction band potentials are then calculated, considering the effects of band-bowing. The resulting maps are significantly different that the low temperature zincblende map and are given in the Supporting Information. The map which includes the effects of radial diffusion is most appropriate to high-temperature-synthesized wurtzite core/shell particles of reference 5. We find that if the product of the diffusion coefficient and time is set to 0.03 nm^2, then the resulting map is very similar to that in reference 5, differing in exciton wavelength by at most a few nanometers. Assuming a 1 hour annealing time,[5] this corresponds to a Se-S interdiffusion coefficient of 5×10^{-4} nm^2 min^{-1}, which is the same order magnitude as reported for Te-Se interdiffusion reported in reference 21. It is important to note that the map shown in figure 4 is not in disagreement with that in reference 5. The two maps are complementary, simply applying to CdSe/CdS particle synthesized under different conditions.

2. Exciton oscillator strengths.

The extinction coefficient spectra in figure 1 are obtained from corresponding absorption spectra by scaling the absorbance to the extinction coefficient at a wavelength where the extinction coefficient can be calculated. The scaling assumes Beer's Law, that the absorbance is proportional the extinction coefficient throughout each spectrum. Extinction coefficients are calculated at a wavelength that is sufficiently short that quantum confinement effects are unimportant, in this case, 350 nm. In the case of core/shell particles, the measured absorption at 350 nm may have a contribution from small, homogeneously nucleated CdS particles. Using the present synthesis, this is typically a small contribution (< 10%) and is corrected for by the comparison of the measured absorption and luminescence excitation spectra. The 350 nm extinction coefficients are calculated from the known particle volumes and compositions, using literature values of the 350 nm optical constants for bulk CdSe

and CdS. This type of procedure is quite standard and has been shown to give reliable assessments of absolute extinction coefficients.[10, 28-30] The real and imaginary components of the 350 nm complex refractive index for CdSe[28, 31] and CdS[31] are $n_{CdSe} = 2.772$, $k_{CdSe} = 0.7726$, and $n_{CdS} = 2.58$, $k_{CdS} = 0.70$. The extinction coefficients at $\lambda = 350$ nm are given by[13]

$$\varepsilon_{QD}(\lambda) = \frac{2\pi N_A}{0.2303\lambda}\frac{2n_{CdSe}k_{CdSe}}{n_s}\left|f_{LF}\right|^2\left(\tfrac{4}{3}\pi r_c^3 + \frac{n_{CdS}k_{CdS}}{n_{CdSe}k_{CdSe}}\tfrac{4}{3}\pi\left((r_c+h)^3 - r_c^3\right)\right) \qquad \text{equation 5.}$$

where r_c is the core radius, h is the shell thickness, $\lambda = 350$ nm and f_{LF} is the local field factor. (Equation 5 uses SI units.) The local field factor is given by[13, 32]

$\left|f_{LF}\right|^2 = \dfrac{9n_s^4}{\left(n_p^2 - k_p^2 + 2n_s^2\right) + 4n_p^2k_p^2}$, where the subscripts p and s refer to the particle and solvent, respectively. Evaluation with the CdSe refractive index and chloroform solvent gives a value of $|f_{LF}|^2 = 0.285$ at 350 nm. Equation 5 gives a 350 nm extinction coefficient of 3.57 x 10^5 l $mol^{-1}cm^{-1}$ for the 2.62 nm CdSe core particles. The core absorption spectrum has a 516.6 nm absorbance that is 0.440 that of the 350 nm absorbance, or 1.57 x 10^5 $M^{-1}cm^{-1}$. It is of interest to compare this extinction coefficient to that reported in reference 13 for the same size particles, which is 1.63 x 10^5 $M^{-1}cm^{-1}$. Reference 13 has all of the lowest exciton absorption peaks corrected for inhomogeneous width, to a HWHM of 0.06 eV. Applying the same correction to the spectrum in figure 1, we get a 516.6 nm extinction coefficient of 1.68 x 10^5 $M^{-1}cm^{-1}$, which is in close agreement with the value reported in reference 13. This is an important check of the internal consistency of these calculations, and confirms the validity of this approach. Using the literature values of 350 nm absorbance coefficients, $n_{CdS}k_{CdS} / n_{CdSe}k_{CdSe} = 0.84$, equation 5 can also be applied to the core/shell spectra. In all cases, integrated extinction coefficients to be used in the evaluation of equation 1 are obtained from fitting the low energy part of these spectra to a superposition of Gaussian peaks and taking the area of the peak corresponding to the $1S_{3/2}$-$1S_e$ transition.

3. Radiative lifetime calculation.

The radiative lifetimes of the 2.62 nm core, and several core/shell particles having the same CdSe cores and different CdS shell thicknesses have been obtained from time-resolved PL measurements. The PL quantum yields of the core/shell particles are very high (> 80%, and usually about 95%) and the PL decays are dominated by a slow component that is taken to be the radiative lifetime. These lifetimes decrease with increasing shell thickness and exciton wavelength, as shown in figure 5. The longest decay component for the core particles is also shown. However, the quantum yield of the core particles is low and the radiationless decay may shorten this decay, compared to the actual radiative lifetime. As such, the measured value of 44.5 ns must be viewed as a lower limit on the actual radiative lifetime. We note that the radiative lifetime decreases with increasing shell thickness and exciton wavelength. This is analogous to what is observed in bare CdSe core particles (where the radiative lifetime decreases with particle size), and the opposite of what is observed in type-II QDs, such as CdTe/CdSe.[10]

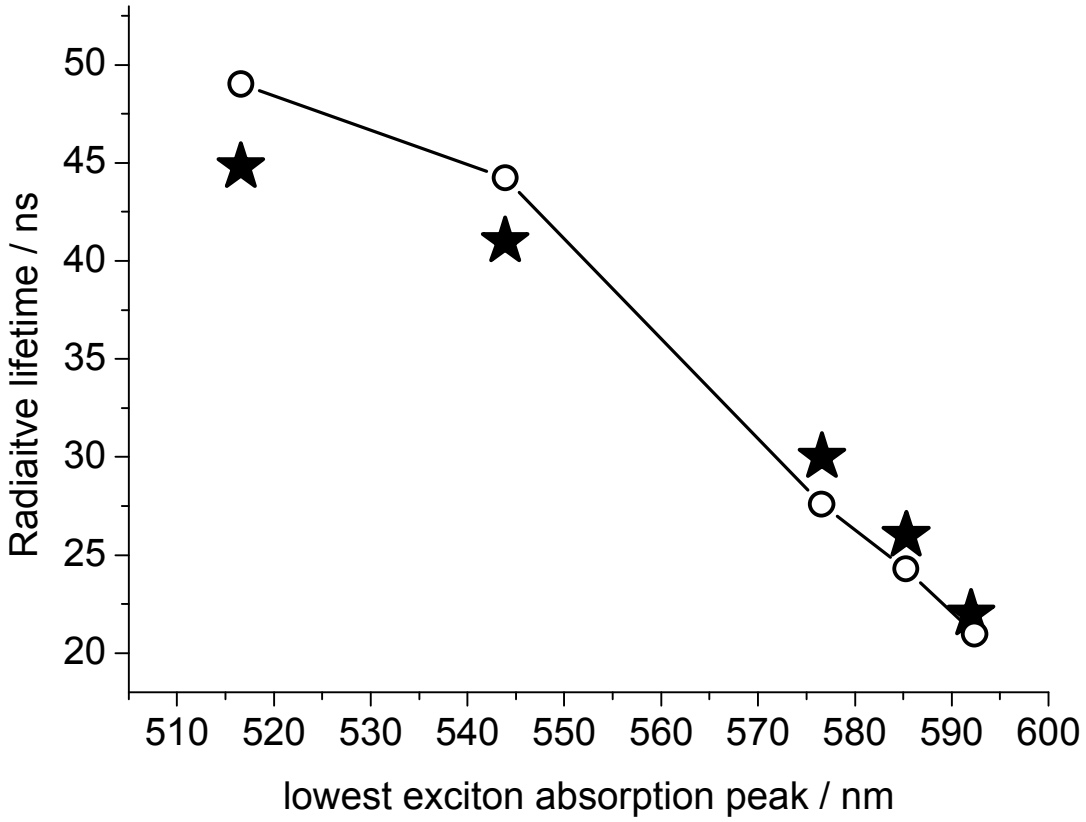

Figure 5. Radiative lifetime as a function of the wavelength of the lowest energy exciton in CdSe/CdS particles. The open circles correspond to radiative lifetimes calculated as described in the text. The 2.64 nm zincblende cores (the 516.6 nm point) have a low QY and the measured lifetime is unreliable.

It is of interest to use equation 1 to compare the measured radiative lifetimes to values calculated from the spectra in figure 1. Although the PL energies and integrated extinction coefficients are easily obtained from figure 1, obtaining accurate C_{fs} values is more complicated. Calculation of C_{fs} amounts to calculating the splittings between the dark and bright angular momentum sublevels[33] and the thermal populations in these sublevels as a function of shell thickness. This calculation also considers the population in the $1P_{3/2}$ hole level, which has only a slight effect.[10, 34] We take the dark-bright splitting to be dominated by the electron-hole exchange interaction, which scales as the reciprocal of the electron-hole separation, 1/r. The electron and hole wavefunctions calculated to obtain the exciton energy map in figure 4 are also used to calculate expectation values of 1/r. These expectation values are obtained by a straight-forward numerical integration over the wavefunctions.[35] Relative 1/r expectation values are used to obtain relative values of E_i compared to those in the core, which are taken from Efros et al.[33] Equation 1 is readily evaluated by using values of C_{fs} obtained from equation 4, the integrated extinctions coefficients, and the exciton energies. A plot of these radiative lifetimes is also shown in figure 5. Very good agreement with the measured decays is obtained for all but the bare CdSe core particles. This may be understood in terms of the fact that the core particles exhibit a lower QY and the long decay

component therefore does not reliably give the radiative lifetime. We note that core radiative lifetime is calculated to be 49 ns, in quantitative agreement with the previously reported value for wurtzite QDs.[10]

It should be noted that this calculational approach uses only the observed spectra and literature data; the calculation of the radiative lifetime has no adjustable parameters. The integrated extinction coefficients of the core/shell particles are obtained directly from the static absorption spectra and the known 350 nm optical constants. The values of C_{fs} for the appropriate sized core particles are from results reported by Efros et al.,[33] and values for the core/shell particles are calculated using calculated expectation values of 1/r. All of the calculated results are in good agreement with radiative lifetimes obtained from time-correlated photon-counting measurements. The Einstein relations (of course) very accurately predict radiative lifetimes. One of the conclusions of this study is very simple: these equations very accurately predict the radiative lifetimes, but only when careful measurements are made and all of the appropriate quantities are correctly evaluated.

These results show that the radiative lifetimes decrease with shell thickness, similar to the size dependence of one-component CdSe quantum dots.[10] This observation is in sharp contrast to what is reported in type-II core/shell QDs, such as CdTe/CdSe.[21] The difference is primarily a result of how the electron-hole overlap varies with shell thickness. In the present case of CdSe/CdS, the band offsets are referred to as type-1½, where the hole is localized in the core and the electron is delocalized throughout the core and shell. Despite the electron delocalization, there remains considerable electron-hole overlap for even rather thick shells. For example, the in the case of the 2.0 nm thick shells, the electron hole overlap is calculated to be $\left|\left\langle \Psi_e \mid \Psi_h \right\rangle\right|^2 = 0.31$. In type-II QDs such as CdTe/CdSe, the band offsets are such that the hole is localized in the core and the electron is localized in the shell. The result is that increasing shell thickness causes the electron-hole overlap to decrease much more rapidly in the type-II, compared to type-1½ QDs. This puts less of the oscillator strength in the $1S_h$-$1S_e$ transition for the type-II QDs, resulting in longer radiative lifetimes.

Experimental Methods.

Optical measurements.

In the time resolved photoluminescence studies, samples were excited with very low intensity 410 nm pulses at 1 MHz from a cavity-dumped frequency-doubled Coherent MIRA laser. The luminescence was imaged through a ¼ m monochromator with a 150 groove/mm grating onto a Micro Photon Devices PDM 50CT SPAD detector. TCPC decays are accumulated using a Becker-Hickle SPC-630 board. The overall temporal response function of the system is about 70 ps.

Quantum yield measurements were made using the same samples as the time resolved luminescence measurements. The static luminescence spectra were measured on a Jobin-Yvon Fluorolog 3 with a CCD detector. Sample spectra were compared with spectra of R6G (assumed to have a 95% QY) taken with the same excitation wavelength and the same absorbance at that wavelength. The wavelength dependence of the CCD detector was taken into account in calculating the nanoparticle quantum yield. This was done by measuring the spectrum of a calibrated tungsten lamp and constructing a detector sensitivity curve.

Chemicals.

Cadmium oxide (CdO, 99.5%), octadecylamine (ODA, 90%), oleylamine (technical grade, 70%), octylamine (99%), sodium diethyldithiocarbamate trihydrate ($NaDDTC \cdot 3H_2O$), cadmium acetate dihydrate ($Cd(Ac)_2 \cdot 2H_2O$), tellurium (Te, 99.8%), trioctylphosphine (TOP, 97%), tributylphosphine (TBP,

97%), octadecene (ODE, 90%), hexane (99.8%), methanol (MeOH, 98%), and toluene (99%) were obtained from Aldrich. Selenium (Se, 99%), oleic acid (OA, 90%), n-octane (98+%) and chloroform ($CHCl_3$, 99.8%) were obtained from Alfa Aesar. ODA was recrystallized from toluene before use. TOP, TBP, and ODE were purified by vacuum distillation. TOPO was purified by repeated recrystallization from acetonitrile. Methanol, chloroform and toluene were purified by distillation from appropriate drying agents. All other chemicals were used as received.

Synthesis and sample preparation.

The zincblende CdSe core nanocrystals are synthesized and purified using slightly modified procedures reported by Nan et al.[2] Zincblende shell deposition occurs from a cadmium-sulfur single precursor, cadmium diethyldithiocarbamate ($Cd(DDTC)_2$), at low temperature (140 - 145 °C). In a typical synthesis, CdO (0.256 g, 0.2 mmol), oleic acid (1 mL) and 4 mL ODE were loaded into a 25 mL three-neck flask. After N_2 bubbling for 2 min, the flask was heated to 250 °C to form a transparent solution and then cooled to 40 °C. Se powder (0.0079 g, 0.1 mmol) was loaded into the flask. The flask was heated to 240 °C under N_2 flow at a heating rate of 40 °C/min. Needle tip aliquots were taken for UV−vis and PL measurements to monitor the size of zincblende CdSe QDs. The particles are then purified by repeated extraction. In these extractions, tributylphosphine (0.2 mL), octylamine (0.2 mL), hexane (3 mL), and methanol (6 mL) were added to the reaction solution at 50 °C and stirred for 2 min. After stirring was turned off, the colorless methanol layer was separated from the top ODE/hexane layer by syringe. This extraction procedure was repeated three times, but TBP was added only the first time. The remaining hexane in the ODE layer was removed by nitrogen bubbling at about 60 °C.

Subsequent CdS shell growth requires the synthesis of ($Cd(DDTC)_2$) for use as the single cadmium and sulfur precursor. In this synthesis, $Cd(Ac)_2 \cdot 2H_2O$ (10 mmol) was dissolved with 100 mL of distilled water in a 400 mL beaker. Into this solution, $NaDDTC \cdot 3H_2O$ (20 mmol) dissolved in 60 mL of distilled water was added dropwise under vigorous stirring. A white precipitate of $Cd(DDTC)_2$ quickly forms. The mixture was stirred for another 20 min after mixing to ensure the reaction was complete. The white precipitate was separated from the solution phase by filtration and washed three times with distilled water. The final product in white powder form was obtained by drying under vacuum overnight. For each shell growth reaction, a 3 mL $Cd(DDTC)_2$-amine-octane solution (0.1 mmol/mL) was prepared by dissolving 0.1227 g of $Cd(DDTC)_2$ in a mixture of octane (1.5 mL), oleylamine (0.45 mL), and octylamine (1.05 mL).

In a typical CdS shell growth reaction, a mixture of ODE (2.0 mL), ODA (20 mg), and oleylamine (1.0 mL) was heated to 60 °C in a three-neck flask under argon flow, and then about 1.0 mL of purified CdSe core solution (containing about 1×10^{-7} mol of nanocrystals estimated by their extinction coefficients) was added to this flask. The amount of precursor solution for each injection was estimated using standard SILAR procedure. In this reaction cycle, addition of the CdS precursor solution is done at 80 °C and growth occurs by heating the solution at a targeted temperature (140 °C for typical synthesis) for about 10 min. This inject-heat-cool cycle was repeated until the desired number of CdS monolayers are obtained. The final reaction solution is purified by extraction with hexane/methanol (v:v~1:1) twice. The non-polar layer is separated and heated under vacuum to remove the residual hexane and methanol. The dried sample is then dissolved in octadecene and ligand exchanged with excess TBP and ODA at 100 °C for about an hour. After ligand exchange, the sample is centrifuged and liquid layer is kept. The particles are precipitated by the addition of anhydrous methanol, dried under vacuum, then dispersed in toluene or chloroform for the spectroscopic measurements.

Acknowledgement.

This work was supported through the Sandia National Labs Solid-State-Lighting Science Energy Frontier Research Center, funded by the U.S. Department of Energy, Office of Basic Energy Sciences. Funding at Sandia was also provided by the Laboratory Research and Development Program. Sandia National Laboratories is a multi-program laboratory managed and operated by Sandia Corporation, a wholly owned subsidiary of Lockheed Martin Corporation, for the U.S. Department of Energy's National Nuclear Security Administration under contract DE-AC04-94AL85000.

*Corresponding author: dfkelley@ucmerced.edu

References.

1.Ghosh, Y.; Mangum, B. D.; Casson, J. L.; Williams, D. J.; Htoon, H.; Hollingsworth, J. A., New Insights into the Complexities of Shell Growth and the Strong Influence of Particle Volume in Nonblinking "Giant" Core/Shell Nanocrystal Quantum Dots. *J. Am. Chem. Soc.* **2012,** 134, 9634−9643.

2.Nan, W.; Niu, Y.; Qin, H.; Cui, F.; Yang, Y.; Lai, R.; Lin, W.; Peng, X., Crystal Structure Control of Zinc-Blende CdSe/CdS Core/Shell Nanocrystals: Synthesis and Structure-Dependent Optical Properties. *J. Am. Chem. Soc.* **2012,** 134, 19685−19693.

3.Embden, J.; Jasieniak, J.; Gómez, D. E.; Mulvaney, P.; Giersig, M., Review of the Synthetic Chemistry Involved in the Production of Core/Shell Semiconductor Nanocrystals. *Aust. J. Chem.* **2007** 60, 457

4.Li, J. J.; Wang, Y. A.; Guo, W.; Keay, J. C.; Mishima, T. D.; Johnson, M. B.; Peng, X., Large-Scale Synthesis of Nearly Monodisperse CdSe/CdS Core/Shell Nanocrystals Using Air-Stable Reagents via Successive Ion Layer Adsorption and Reaction. *J. Am. Chem. Soc.* **2003,** 125, 12567.

5.Embden, J. v.; Jasieniak, J.; Mulvaney, P., Mapping the Optical Properties of CdSe/CdS Heterostructure Nanocrystals: The Effects of Core Size and Shell Thickness. *J. Am. Chem. Soc.* **2009,** 131, 14299.

6.García-Santamaría, F.; Chen, Y.; Vela, J.; Schaller, R. D.; Hollingsworth, J. A.; Klimov, V. I., Suppressed Auger Recombination in "Giant" Nanocrystals Boosts Optical Gain Performance. *Nano Lett.* **2009,** 2, 3482.

7.Guo, Y.; Marchuk, K.; Sampat, S.; Abraham, R.; Fang, N.; Malko, A. V.; Vela, J., Unique Challenges Accompany Thick-Shell CdSe/nCdS (n > 10) Nanocrystal Synthesis. *J. Phys. Chem. C* **2012,** 116, 2791-2800.

8.Smith, A. M.; Mohs, A. M.; Nie, S., Tuning the optical and electronic properties of colloidal nanocrystals by lattice strain. *Nature Nanotechnology* **2009,** 4, 56 - 63.

9.Gong, K.; Kelley, D. F., A Predictive Model of Shell Morphology in CdSe/CdS Core/Shell Quantum Dots. *J. Chem. Phys.* **2014**, in press.

10.Gong, K.; Zeng, Y.; Kelley, D. F., Extinction Coefficients, Oscillator Strengths, and Radiative Lifetimes of CdSe, CdTe, and CdTe/CdSe Nanocrystals. *J. Phys. Chem. C* **2013,** 117, 20268-20279.

11.Kelley, A. M., *Condensed-Phase Molecular Spectroscopy and Photophysics*. Wiley: Hoboken, NJ, 2013.

12.Strickler, S. J.; Berg, R. A., Relationship between Absorption Intensity and Fluorescence Lifetime of Molecules. *J. Chem. Phys.* **1962,** 37, 814 - 822.

13.Jasieniak, J.; Smith, L.; Embden, J. v.; Mulvaney, P.; Califano, M., Re-examination of the Size-Dependent Absorption Properties of CdSe Quantum Dots. *J. Phys. Chem. C* **2009,** 113, 19468 - 19474.

14.Yu, P. Y.; Cardona, M., *Fundamentals of Semiconductors*. third ed.; Springer: Berlin, 2001.

15.Norris, D. J., Electronic Structure in Semiconductor Nanocrystals: Optical Experiment. In *Nanocrystal Quantum Dots*, 2'd ed.; Klimov, V. I., Ed. CRC Press: 2010.

16.Saada, A. S., *Elasticity Theory and Applications*. Permagon Press: New York, 1974.

17.Rockenberger, J.; Troger, L.; Rogach, A. L.; Tischer, M.; Grundmann, M.; Eychmuller, A.; Weller, H., The contribution of particle core and surface to strain, disorder and vibrations in thiol-capped CdTe nanocrystals. *J. Chem. Phys.* **1998,** 108, (18), 7807-7815.

18.West, A. R., *Basic Solid State Chemistry*. Wiley Chichester, 1988.

19.Shan, W.; Walukiewicz, W.; Ager, J. W., III; Yu, K. M.; Wu, J.; Haller, E. E., Pressure dependence of the fundamental band-gap energy of CdSe. *Appl. Phys. Lett.* **2004,** 84, (1), 67-69.

20.San-Miguel, A.; Polian, A.; Itie, J. P.; Marbuef, A.; Triboulet, R., Zinc Telluride Under High Pressure: An X-Ray Absorption Study. *High Pressure Research* **1992,** 10, 412.

21.Cai, X.; Mirafzal, H.; Nguyen, K.; Leppert, V.; Kelley, D. F., The Spectroscopy of CdTe/CdSe type-II Nanostructures: Morphology, Lattice Mismatch and Band-Bowing Effects. *J. Phys. Chem. C* **2012,** 116, 8118 - 8127.

22.Talapin, D. V.; Koeppe, R.; Gtzinger, S.; Kornowski, A.; Lupton, J. M.; Rogach, A. L.; Benson, O.; Feldmann, J.; Weller, H., Highly Emissive Colloidal CdSe/CdS Heterostructures of Mixed Dimensionality. *Nano Letters* **2003,** 3, 1677.

23.Steiner, D.; Dorfs, D.; Banin, U.; Della Sala, F.; Manna, L.; Millo, O., Determination of Band Offsets in Heterostructured Colloidal Nanorods Using Scanning Tunneling Spectroscopy. *Nano Lett.* **2008,** 8, 2954.

24.Wu, K.; Rodrıguez-Cordoba, W. E.; Liu, Z.; Zhu, H.; Lian, T., Beyond Band Alignment: Hole Localization Driven Formation of Three Spatially Separated Long-Lived Exciton States in CdSe/CdS Nanorods. *ACS Nano* **2013,** 7, 7173.

25.Bailey, R. E.; Nie, S., Alloyed Semiconductor Quantum Dots: Tuning the Optical Properties without Changing the Particle Size. *J. Am. Chem. Soc.* **2003,** 125, 7100.

26.Regulacio, M. D.; Han, M.-Y., Composition-Tunable Alloyed Semiconductor Nanocrystals. *Acc. Chem. Res.* **2010,** 43, 621–630.

27.Wei, S.-H.; Zhang, S. B.; Zunger, A., First-principles calculation of band offsets, optical bowings, and defects in CdS, CdSe, CdTe, and their alloys. *J. Appl. Phys* **2000,** 87, 1304.

28.Leatherdale, C. A.; Woo, W.-K.; Mikulec, F. V.; Bawendi, M. G., On the Absorption Cross Section of CdSe Nanocrystal Quantum Dots *J. Phys. Chem. B.* **2002,** 106, 7619 - 7622.

29.Capek, R. K.; Moreels, I.; Lambert, K.; Muynck, D. D.; Zhao, Q.; Tomme, A. V.; Vanhaecke, F.; Hens, Z., Optical Properties of Zincblende Cadmium Selenide Quantum Dots. *J. Phys. Chem. C* **2010,** 114, 6371 - 6376.

30.de Mello Donega, C.; Koole, R., Size Dependence of the Spontaneous Emission Rate and Absorption Cross Section of CdSe and CdTe Quantum Dots. *J. Phys. Chem. C* **2009,** 113, 6511 - 6520.

31.Palik, E. D., *Handbook of Optical Constants of Solids*. Academic Press: 1998; Vol. II.

32.Ricard, D.; Chanassi, M.; Schanne-Klein, M., Dielectric confinement and the linear and nonlinear optical properties of semiconductor-doped glasses. *Opt. Commun.* **1996,** 108, 311.

33.Efros, A. L.; Rosen, M.; Kuno, M.; Nirmal, M.; Norris, D. J.; Bawendi, M., Band-edge exciton in quantum dots of semiconductors with a degenerate valence band: Dark and bright exciton states. *Phys. Rev. B* **1996,** 54, 4843 - 4856.

34.Efros, A. L.; Rosen, M., Quantum size level structure of narrow-gap semiconductor nanocrystals: Effect of band coupling. *Phys. Rev. B* **1998,** 58, 7120 - 7135.

35.Jackson, *Classical Electrodynamics*. 2'd ed.; Wiley: New York, 1975.